



Cite this: *Environ. Sci.: Nano*, 2018, 5, 2590

# Influence of light wavelength on the photoactivity, physicochemical transformation, and fate of graphene oxide in aqueous media†

Tingting Du,<sup>a</sup> Adeyemi S. Adeleye,<sup>b</sup> ‡<sup>b</sup> Tong Zhang,<sup>a</sup> Chuanjia Jiang,<sup>a</sup> Min Zhang,<sup>a</sup> Huihui Wang,<sup>a</sup> Yao Li,<sup>b</sup> \*<sup>a</sup> Arturo A. Keller<sup>\*b</sup> and Wei Chen<sup>b</sup>

The rapidly increasing production and application of graphene oxide (GO) calls for much-needed attention to aspects related to the environmental implications of this unique nanomaterial. To date, very little is known about the transformation of GO when exposed to electromagnetic radiation at different wavelengths, which can occur in natural water systems. This study explored the changes in the physicochemical properties of GO when exposed to the UV and visible wavelength ranges of simulated solar light. Irradiation, especially under UV light, led to remarkable changes in the surface oxygen (O)-functionalities of GO, and cleavage of GO's graphitic bond. The carbon/oxygen (C/O) ratio of GO increased by 41% and 31% after irradiation with simulated solar light and UV irradiation, respectively. Visible light also changed the morphology of GO, but the C/O ratio only increased by 5.5%. The formation of hydroxyl radicals (<sup>•</sup>OH), superoxide (O<sub>2</sub><sup>•-</sup>) and singlet oxygen (<sup>1</sup>O<sub>2</sub>) by GO was observed during irradiation with both UV and visible lights, but the proportions were different. <sup>1</sup>O<sub>2</sub> was primarily formed during visible light irradiation, while O<sub>2</sub><sup>•-</sup> and <sup>•</sup>OH were mostly formed under UV light. <sup>•</sup>OH hydroxylated GO, which mainly resulted in the decomposition of GO. The changes in O-containing functional groups on GO by irradiation influenced the colloidal stability of GO in aqueous media, but the physical wrinkle on GO surface may strongly affect its interactions with other organic materials.

Received 4th June 2018,  
Accepted 11th September 2018

DOI: 10.1039/c8en00593a

rsc.li/es-nano

## Environmental significance

The applications of graphene oxide (GO) are leading to increasing environmental release of these novel materials. As a reactive nanomaterial, it is unlikely that GO will maintain its pristine form in the environment; instead, GO can undergo substantial transformation, *e.g.* under the irradiation of sunlight. However, the full band of solar light will be filtered or partially minimized in natural water systems, *e.g.* UV light could be filtered out with increasing water depth. It is unclear how the physicochemical properties of GO will change in natural waters when exposed to lights with different wavelength ranges (*i.e.*, UV or visible light). Thus, knowledge on the wavelength-dependent photo-transformation of GO is necessary to better understand the fate and transport of GO nanomaterials in the environment.

## 1 Introduction

Graphene oxide (GO) is a structural analog of graphene, and it possesses abundant oxygen (O)-containing functionalities

such as epoxide (C–O–C), hydroxyl (C–OH), carbonyl (C=O), and carboxyl groups (O–C=O) covalently bound to either its basal planes (C–O–C and C–OH groups) or edges (C=O and O–C=O groups).<sup>1–3</sup> GO can be stabilized in aqueous media as colloidal agglomerates because of its functionalization, and it is more reactive in water than other carbon nanomaterials, such as C<sub>60</sub> and carbon nanotubes.<sup>4,5</sup> GO is increasingly being proposed for commercial products, such as nanopaints, polymer composites, functional coatings, and water treatment nanohybrids, which could lead to release of the nanomaterial into the environment.<sup>6–9</sup> Thus, it is expected that wastes containing GO will be generated and released into the environment, and may accumulate in landfills or surface waters.

As a reactive nanoparticle, it is unlikely that GO will maintain its pristine form in the environment. The

<sup>a</sup> College of Environmental Science and Engineering, Ministry of Education Key Laboratory of Pollution Processes and Environmental Criteria, Tianjin Key Laboratory of Environmental Remediation and Pollution Control, Nankai University, 38 Tong Yan Road, Tianjin 300350, China.

E-mail: hkllyao@nankai.edu.cn; Fax: 86 22 2350 1117; Tel: 86 22 2350 1117

<sup>b</sup> Bren School of Environmental Science and Management, University of California, Santa Barbara, California 93106, USA. E-mail: keller@bren.ucsb.edu;

Fax: 86 22 2350 1117; Tel: 86 22 2350 1117

† Electronic supplementary information (ESI) available. See DOI: 10.1039/c8en00593a

‡ Current address: Department of Civil and Environmental Engineering, University of California, Irvine, CA 92697, United States.

physicochemical characteristics of GO can change substantially when it is exposed to the environment *via* several natural or engineered processes.<sup>10–16</sup> In the environment, solar irradiation is the most common factor that may induce or affect the transformation of GO, which can change the chemical characteristics as well as the morphology of pristine GO. Several studies indicated that GO could be reduced and decomposed in the presence of simulated sunlight irradiation,<sup>17–19</sup> producing CO<sub>2</sub> and other small sized particles, such as polycyclic aromatic hydrocarbons (PAHs). However, most of these studies only considered the transformation of GO under full-spectrum simulated solar light, while no study has focused on the transformation of GO under light of different wavelengths. In natural waters, the UV fraction of solar light will be significantly filtered with increasing water depth,<sup>20–22</sup> and the remaining visible light will be mainly responsible for the transformation of GO. In addition, UV light, which is frequently used in wastewater treatment systems,<sup>23</sup> can directly change GO's physicochemical characteristics within wastewater treatment processes. The above-mentioned light conditions may induce different patterns of GO transformation and possibly change the environmental fate of GO transformation products.<sup>17</sup> Besides, GO may undergo photocatalytic reactions in water to produce different types of reactive oxygen species (ROS). In a recent study where GO was exposed to solar irradiation, we demonstrated the production of hydroxyl radicals (<sup>•</sup>OH), superoxide radical anions (O<sub>2</sub><sup>•-</sup>) and singlet oxygen (<sup>1</sup>O<sub>2</sub>) by GO.<sup>24</sup> However, the specific effect of each distinct fraction (of the solar spectrum) is still unknown, and some ROS, such as <sup>•</sup>OH, have high reactivity and can generate highly oxidizing organic radicals.<sup>25</sup> The mechanism and effects of the produced ROS on the transformation of GO are also unclear.

In summary, the objectives of the study were to (1) investigate the physicochemical transformation of GO under the UV (290–420 nm) and visible wavelength range (>420 nm), (2) explore the ratio of the ROS formed under different light wavelengths and their impacts on GO transformation, and (3) determine the influence of GO transformation under UV and visible light on its environmental fate and interactions.

## 2 Experimental

### 2.1 Materials and stock preparation

Graphene oxide (GO) nanoparticles (>99%) were purchased from Plannano Materials Tech. Co. (Tianjin, China) and used as received. The nanomaterials were synthesized using a modified Hummers method, according to the information provided by the manufacturer.<sup>26</sup> To prepare GO stock suspensions, 90 mg of pristine GO nanosheets was added into 300 mL of deionized (DI) water in a 500 mL Erlenmeyer flask and then ultrasonicated at 100 W for 4 h using a Vibra-Cell VCX800 sonicator (Sonics & Materials, USA). A uniform dark-brown suspension was obtained and kept in the dark at 4 °C until use. The GO in the suspension had an average hydrodynamic parameter of 129.5 ± 23.2 nm, according to dynamic

light scattering (DLS) analysis (Zetasizer Nano ZS90, Malvern Instruments, Worcestershire, UK).

Methanol, acetonitrile, toluene, acetone, chloroform, furfuryl alcohol (FFA), terephthalic acid (TA), phenanthrene, and 1-naphthol were purchased from Sigma-Aldrich (St. Louis, USA).

### 2.2 Set-up of photochemistry experiments

The photochemistry set-up was similar to the one used previously.<sup>24</sup> In summary, a photochemical reaction apparatus (XPA-7, Xu Jiang Machine Plant, Nanjing, China) connected to an 800 W xenon lamp was used as the light source, and a 290 nm cutoff filter was used to adjust the light irradiation to simulate the solar spectrum typical of the real environment ( $\lambda > 290$  nm). A 420 nm cutoff filter was used to allow only visible light ( $\lambda > 420$  nm), and another filter was used to allow only UV light ( $\lambda = 290$ –420 nm). Fig. S1† shows a comparison of the spectra for these different wavelengths and natural solar irradiation (collected on May 28, 2015).

The concentration of GO used for the experiment was 10 mg L<sup>-1</sup>. The photochemistry experiment was conducted in DI water in order to simplify the system enough for us to clearly decipher the role of the different light wavelengths on the photo-transformation of GO. The reaction was carried out in a 60 mL grinding-mouth transparent quartz tube, and a 1.5 cm magnetic stirrer was used for mixing. The quartz tubes were submerged in a thermostat-controlled water bath (25 °C) during irradiation experiments. Samples were irradiated for 8 h per day for 3 days, making a total of 24 h. All the samples, including GO (the pristine nanomaterial not exposed to any irradiation), GO<sub>full</sub> (GO with full-spectrum simulated solar irradiation,  $\lambda > 290$  nm), GO<sub>UV</sub> (GO with only UV light irradiation,  $\lambda = 290$ –420 nm) and GO<sub>vis</sub> (GO with visible light irradiation,  $\lambda > 420$  nm), were prepared for characterization.

### 2.3 Graphene oxide characterization

GO was characterized as pristine particles and after irradiation treatments. For post-irradiation characterization, dry GO particles were obtained from the treated GO suspensions *via* freeze-drying. The chemical composition and functional groups of pristine and photo-treated GO (GO<sub>full</sub>, GO<sub>UV</sub> and GO<sub>vis</sub>) were characterized *via* X-ray photoelectron spectroscopy (XPS, using a PHI 5000 VersaProbe, Japan), Fourier transform infrared (FTIR) transmission spectroscopy (110 Bruker TENSOR 27 apparatus, Germany), and Raman spectroscopy (Renishaw InVia Raman spectrometer, England). The UV-visible absorbance spectra of the GO suspensions were obtained with a UV-2401 spectrophotometer (Shimadzu Scientific Instruments, USA). The morphology of GO was characterized by atomic force microscopy (AFM, MMAFM/STM, D3100M, Digital Ltd., USA), scanning electron microscopy (SEM, FEI Nova NanoSEM 430, The Netherlands) and transmission electron microscopy (TEM, FEI Tecnai G2100 F-20, The Netherlands).

## 2.4 Reactive oxygen species (ROS) detection

The steady-state concentrations of  $^1\text{O}_2$  were determined indirectly by monitoring the concentrations of FFA, as explained in a previous study<sup>24</sup> and summarized here (eqn (1) and (2)). The concentration of the GO suspension used was  $10 \text{ mg L}^{-1}$ , and a known amount of FFA standard water stock solution was injected into the quartz container with a micro-syringe to achieve a FFA concentration of  $50 \text{ }\mu\text{M}$ . Samples were collected from the quartz container (after irradiation for 0, 1, 2, 4, 6, 16, and 24 h) using a 1 mL glass syringe and passed through  $0.22 \text{ }\mu\text{m}$  filters to remove GO particles prior to high-performance liquid chromatography (HPLC) analysis.  $[^1\text{O}_2]_{\text{ss}}$  was determined by dividing the observed FFA degradation rate by the reaction rate constant of FFA with  $^1\text{O}_2$  and the residual concentration of FFA (which was determined *via* HPLC using a Waters e2695 (Waters Technology, USA) equipped with a symmetry reversed phase  $\text{C}_{18}$  column ( $4.6 \times 150 \text{ mm}$ )). FFA was detected with a Waters 2489 UV/visible detector at a wavelength of 219 nm; the mobile phase used was 40% acetonitrile and 60%  $\text{H}_2\text{O}$  with a flow rate of  $1.0 \text{ mL min}^{-1}$ .



$$\frac{d[\text{FFA}]}{dt} = -k_{\text{FFA},^1\text{O}_2} [\text{FFA}] [^1\text{O}_2]_{\text{ss}} \quad (2)$$

where  $k_{\text{FFA},^1\text{O}_2} = 8.3 \times 10^7 \text{ M}^{-1} \text{ s}^{-1}$ .<sup>27</sup>

The steady-state concentrations of  $\text{O}_2^{\cdot-}$  were measured with a chemiluminescent probe (2-methyl-6-[*p*-methoxyphenyl]-3,7-dihydroimidazo[1,2-*a*]pyrazin-3-one (MCLA)), which can selectively react with  $\text{O}_2^{\cdot-}$ . The detailed procedure was described by Adeleye *et al.* (2018).<sup>24</sup> A  $200 \text{ }\mu\text{M}$  MCLA stock solution was prepared and subsequently frozen at  $4 \text{ }^\circ\text{C}$ . The analytical reagent contained  $1.0 \text{ }\mu\text{M}$  MCLA buffered with  $0.05 \text{ M}$  sodium acetate, and the final pH of this reagent was adjusted to 5.5 using quartz-distilled HCl. During the measurement, the analytical reagent and GO/ $\text{GO}_{\text{full}}$ / $\text{GO}_{\text{UV}}$ / $\text{GO}_{\text{vis}}$  ( $10 \text{ mg L}^{-1}$ ) were pumped at a 1:1 (v/v) ratio into a purpose-built flow injection analysis (FIA) system (Waterville Analytical, Waterville, ME, US). The reaction between  $\text{O}_2^{\cdot-}$  and MCLA resulted in a chemiluminescence signal at 455 nm, which was detected using a photomultiplier.

Terephthalic acid (TA) was used to measure the steady-state concentrations of  $\cdot\text{OH}$ . 2-Hydroxy-terephthalic acid (2HTA) is generated during the reaction of TA with  $\cdot\text{OH}$ , and the reaction is unaffected by the presence of other reactive species such as  $\text{O}_2^{\cdot-}$ ,  $\text{HO}_2^{\cdot}$ , and  $\text{H}_2\text{O}_2^{\cdot}$ .<sup>28</sup> 2HTA was analyzed *via* HPLC and detected with a Waters 2475 fluorescence detector at an excitation wavelength of 315 nm and an emission wavelength of 425 nm; the mobile phase consisted of 65% trifluoroacetic acid buffer (0.05% v/v) and 35% acetonitrile (v/v) at a flow rate of  $1.0 \text{ mL min}^{-1}$ .

*Tert*-butanol (*t*-BuOH) was used to eliminate  $\cdot\text{OH}$  radicals in the suspension.  $10 \text{ mM}$  *t*-BuOH was mixed into the GO samples before irradiation and then the irradiated GO samples were collected for further characterization.<sup>29,30</sup>

## 2.5 Influence of photo-treatment on GO fate

To understand how the exposure of GO to different light wavelengths will influence the environmental fate of the nanomaterial, additional studies were carried out to determine changes in the hydrodynamic diameter ( $D_h$ ), agglomeration kinetics, and zeta ( $\zeta$ ) potential of the photo-treated GO suspensions at  $25 \text{ }^\circ\text{C}$  using the Zetasizer. Furthermore, changes in the adsorption properties of GO were also characterized.

**2.5.1 Zeta ( $\zeta$ ) potential measurements.** To determine the effect of exposure of GO to different wavelengths of light on the surface charge of the nanomaterial, the  $\zeta$  potential of the suspensions of GO,  $\text{GO}_{\text{full}}$ ,  $\text{GO}_{\text{UV}}$ , and  $\text{GO}_{\text{vis}}$  ( $10 \text{ mg L}^{-1}$  each) was determined using the Zetasizer. The  $\zeta$  potential measurements were carried out between pH 3 and pH 11 (adjusted with  $0.1 \text{ mM}$  NaOH or HCl). Each measurement was conducted over 15 seconds, and a total of 3 replicates were measured per treatment.

**2.5.2 Agglomeration experiments.** The changes in the hydrodynamic diameter ( $D_h$ ) of the GO agglomerate with time was measured with time-resolved dynamic light scattering (TR-DLS), at increasing concentrations of NaCl, with or without  $5 \text{ mg L}^{-1}$  Suwannee River humic acid (SRHA).<sup>4,31</sup> In these experiments, a known amount of GO stock suspension was pipetted into a glass vial containing either DI water or an electrolyte solution (the pH was adjusted to 7 with  $0.1 \text{ mM}$  NaOH or HCl, if needed) to achieve a GO or treated GO concentration of  $10 \text{ mg L}^{-1}$ . Then, the vial was capped and immediately vortexed for 5 s and 1 mL of the suspension was pipetted into a polystyrene cuvette, which was placed in the Zetasizer's sample chamber for TR-DLS analysis. The autocorrelation function was allowed to accumulate for 15 s during the agglomeration study and the  $D_h$  measurements were conducted over a period of 60 min. As shown in eqn (3), the initial agglomeration rate constant of GO ( $k$ ) reflects doublet formation and is proportional to the initial rate of increase in  $D_h$  with time ( $t$ ) and the inverse of the GO concentration ( $N_0$ ):<sup>32–35</sup>

$$k \propto \frac{1}{N_0} \left( \frac{dD_h(t)}{dt} \right)_{t \rightarrow 0} \quad (3)$$

The particle attachment efficiency ( $\alpha$ ) was used to quantify the GO agglomeration kinetics, and it was calculated by normalizing the measured  $k$  at a given ionic strength (with or without HA) with the agglomeration rate constant measured under diffusion limited (fast) conditions, as shown in eqn (4):

$$\alpha = \frac{1}{W} = \frac{k}{k_{\text{fast}}} = \frac{\frac{1}{N_0} \left( \frac{dD_h(t)}{dt} \right)_{t \rightarrow 0}}{\frac{1}{(N_0)_{\text{fast}}} \left( \frac{dD_h(t)}{dt} \right)_{t \rightarrow 0, \text{fast}}} \quad (4)$$

The diffusion-limited (DLCA) and reaction-limited (RLCA) clustering agglomeration regimes, and thus, the critical coagulation concentrations (CCCs), can be identified in a plot of

$\log_{10}[\text{NaCl}]$  versus  $\log_{10} \alpha$ . DLCA occurs when the attachment efficiency between particles is close to unity, whereas RLCA dominates at very low attachment efficiencies.<sup>36</sup> CCC is the point of intersection between DLCA and RLCA.

**2.5.3 Adsorption experiments.** Adsorption experiments were carried out by using a previously developed method.<sup>37</sup> Aliquots of pristine and photo-treated GO stock suspensions ( $250 \text{ mg L}^{-1}$ ) were diluted with DI water to achieve a final concentration of  $50 \text{ mg L}^{-1}$  GO. Phenanthrene (a representative nonpolar, nonionic aromatic compound) and 1-naphthol (a model polar aromatic compound) were selected as the model contaminants. The detailed procedure for the adsorption isotherm experiments is described in the ESI.† The concentrations of contaminants were determined using a Waters e2695 HPLC connected to a Waters 2475 fluorescence detector. The HPLC was equipped with a Waters  $\text{C}_{18}$  ( $4.6 \times 150 \text{ mm}$ ) reverse phase column, and the mobile phase consisted of 80% acetonitrile and 20% water (flow rate  $1 \text{ mL min}^{-1}$ ). For the Waters 2475 fluorescence detector, the excitation wavelength was 250 nm, and the emission wavelength was set at 364 nm. The column incubator temperature was set to  $25 \text{ }^\circ\text{C}$ .

## 3 Results and discussion

### 3.1 Characterization of pristine and photo-treated GO

The chemical transformation of GO upon irradiation under different light wavelengths was evaluated. The XPS spectra of pristine GO,  $\text{GO}_{\text{full}}$ ,  $\text{GO}_{\text{UV}}$  and  $\text{GO}_{\text{vis}}$  are provided in Fig. 1a–d and the associated quantitative data are summarized in Table 1. The binding energy level and FWHM values of GOs are summarized in Table S1.† The carbon/oxygen (C/O) ratio increased by 41% from 1.80 for GO to 2.54 for  $\text{GO}_{\text{full}}$ , which indicates that reduction of GO occurred during the 24 h irradiation under full-spectrum simulated solar light. After irradiation by UV and visible light, the C/O ratio increased by 31% and 5.5%, respectively, which also confirmed the loss of O-functional groups (*i.e.*, reduction of GO) when GO was exposed to irradiation in the UV and visible light regions. In addition, the relative abundance of the different O-functional groups on the surface of GO changed remarkably upon irradiation at the different irradiation wavelengths, as shown by the deconvolution of the XPS C 1s spectra (summarized in Table 1).<sup>38</sup> The relative abundance of GO's aromatic C–C/

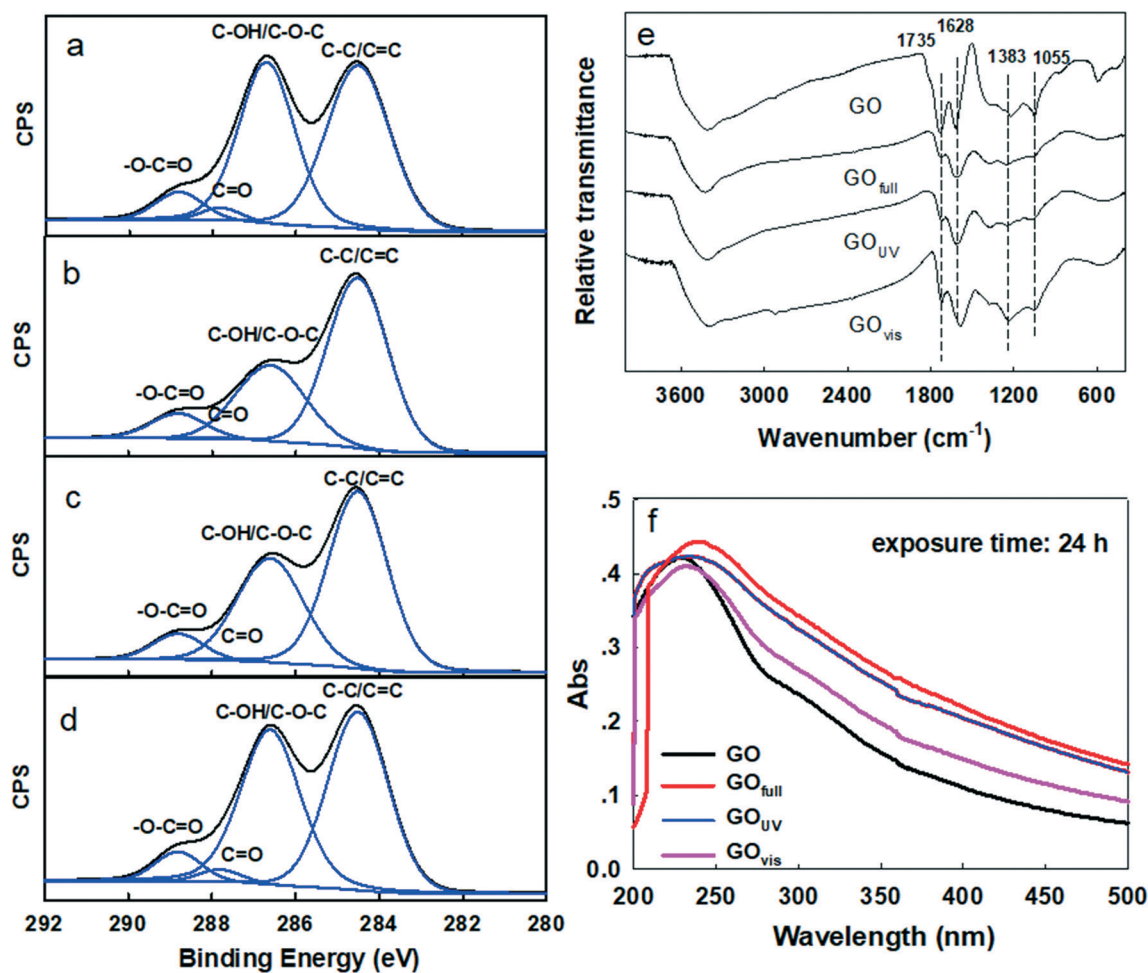


**Fig. 1** Photo-transformation of GO. High resolution C 1s XPS spectra of (a) pristine GO, (b) GO exposed to the full solar spectrum ( $\lambda > 290 \text{ nm}$ ), (c) GO exposed to UV light ( $\lambda = 290\text{--}420 \text{ nm}$ ), and (d) GO exposed to visible light ( $\lambda > 420 \text{ nm}$ ). Changes in GO after exposure to light of different wavelengths were also determined via (e) FTIR spectroscopy and (f) UV-vis absorbance spectroscopy.

**Table 1** XPS quantitative data of GO, GO<sub>full</sub>, GO<sub>UV</sub> and GO<sub>vis</sub>

Sample ID	C (atom %)				Total C (atom %)	Total O (atom %)	C/O ratio
	C-C/C=C	C-OH/C-O-C	C=O	O-C=O			
GO	45.16	43.71	4.77	6.36	64.29	35.72	1.80
GO <sub>full</sub>	62.42	25.14	3.14	9.30	71.76	28.24	2.54
GO <sub>UV</sub>	57.13	32.62	3.06	7.19	70.25	29.74	2.36
GO <sub>vis</sub>	49.15	40.26	4.30	6.29	65.47	34.53	1.90

C=C group (binding energy [BE] = 284.6 eV) increased from 45.16% (in pristine GO) to 62.42%, 57.13% and 49.15% after irradiation with full-spectrum solar, UV and visible light, respectively. Irradiation, especially with full-spectrum solar and UV light, resulted in a considerable decrease in the C-O-C/C-OH (BE = 286.6 eV) and C=O (BE = 287.8 eV) groups, while the relative abundance of the O-C=O group (BE = 288.8 eV) increased. The changes in GO's functional groups were minimal when irradiated by visible light alone.

Changes in the surface chemistry of GO upon irradiation with different electromagnetic wavelengths were further characterized by other spectroscopic techniques including FTIR and UV-vis absorption spectroscopy (Fig. 1e and f). The FTIR spectrum of pristine GO exhibited four characteristic peaks located at 1055, 1383, 1628 and 1735 cm<sup>-1</sup>, corresponding to C-O-C stretching, a C-O group, O-C=O stretching, and C=O stretching, respectively.<sup>39-41</sup> The C-O, C-O-C and C=O groups decreased slightly after irradiation with the full solar spectrum and UV light. The characteristic absorbance peak of GO at 230 nm was observed for pristine GO, which can be ascribed to  $\pi-\pi^*$  transitions in small electronically conjugated domains present in the material.<sup>42</sup> The characteristic absorbance peak however shifted to 240 nm in GO<sub>UV</sub> and 250 nm in GO<sub>full</sub> (after 24 h exposure), which indicates an increase in the electronically conjugated domain, resulting from the reduction of GO. The time-series UV-vis spectra of irradiated GO showed progressive red-shifting of the GO peak at 230 nm when exposed to the full solar spectrum and UV irradiation but no substantial shift under visible light irradiation for up to 32 h (Fig. S2†). In addition, the peak at around 300 nm, originating from the  $n-\pi^*$  transitions of the O-functionalities, was clearly observed in pristine GO.<sup>3</sup> The intensity of the peak decreased in GO<sub>vis</sub> and was not observed in GO<sub>UV</sub> and GO<sub>full</sub>, indicating reduction of GO under those conditions. The UV-vis absorbance includes the absorbance of unreacted GO, light-transformed GO and any other photoreaction products. The increase in absorbance (especially when GO was exposed to the full spectrum and UV) thus shows that light-absorbing photoproducts were formed upon irradiation of GO. In addition, the increased peak intensity at around 254 nm, which reflects aromaticity, may also indicate an increasing degree of graphitization of GO after its reduction by irradiation.

Changes in the morphology of GO after exposure to light of different irradiation wavelengths were also examined. Untreated GO nanosheets appeared smooth, with some minimal wrinkles under the TEM (Fig. 2a) and SEM (Fig. 2e). The nanomaterials, however, appeared broken up into smaller-

sized sheets upon exposure to full-spectrum solar (Fig. 2b and f) and UV lights (Fig. 2c and g). The GO samples exposed to visible light were not remarkably broken up, but more wrinkles were observed in the TEM micrographs (Fig. 2d and h). Breaking up of GO sheets into smaller pieces upon photo-treatment with full-spectrum solar and UV light was confirmed by AFM analysis, which also showed no remarkable difference in size distribution between pristine GO and GO exposed to visible light. The Raman spectra of the GO samples (Fig. S3†) indicated an increase in the  $I_D/I_G$  ratio (the ratio of the intensity of the D band (around 1350 cm<sup>-1</sup>) to that of the G band (around 1580 cm<sup>-1</sup>)) after 24 h irradiation for all the samples, especially GO<sub>UV</sub>. Since  $I_D/I_G$  is a measure of the average size of the in-plane sp<sup>2</sup> domains and molecular defects,<sup>43</sup> the results showed that more defect sites were formed on the graphenic sheets upon irradiation for all light sources. The physical appearance of the GO suspension also changed when it was exposed to different irradiation wavelengths for 24 h (Fig. S4†). Specifically, the color of GO darkened strongly upon irradiation with the full solar spectrum and UV light. The GO suspension was only slightly darker upon its exposure to visible light for 24 h. Time series experiments showed that the darkening of the GO suspension became stronger over time upon exposure to all three irradiation types (Fig. S5†). In general, the intensity of the GO darkening observed was GO<sub>full</sub> > GO<sub>UV</sub> >> GO<sub>vis</sub> (Fig. S5†). Darkening of GO is mainly due to the reduction of GO functional groups by the irradiation, which may destroy some chromophore units (such as C-OH and C=O groups on the graphitic carbon).<sup>17,44</sup>

In general, characterization of GO, GO<sub>full</sub>, GO<sub>UV</sub>, and GO<sub>vis</sub> showed that irradiation strongly changed the physicochemical properties of the nanomaterials and the changes were correlated with the wavelength, and thus, the photon energy, of the irradiation. The characterization data showed that UV and full spectrum light cause remarkable physicochemical changes in GO, which is mainly because the energy of the photons of UV exceeds the bandgap of the GO domains. In contrast, the photons of visible light do not have as much energy. Thus, more substantial changes in the physicochemical properties of GO were observed in GO<sub>full</sub> (which included irradiation in the UV region) and GO<sub>UV</sub> compared to GO<sub>vis</sub>. The XPS and FTIR spectra indicated that the reduction of GO by irradiation was mostly due to UV photons, while visible light only generated modest changes in GO's functional groups. The TEM, SEM and AFM micrographs clearly showed

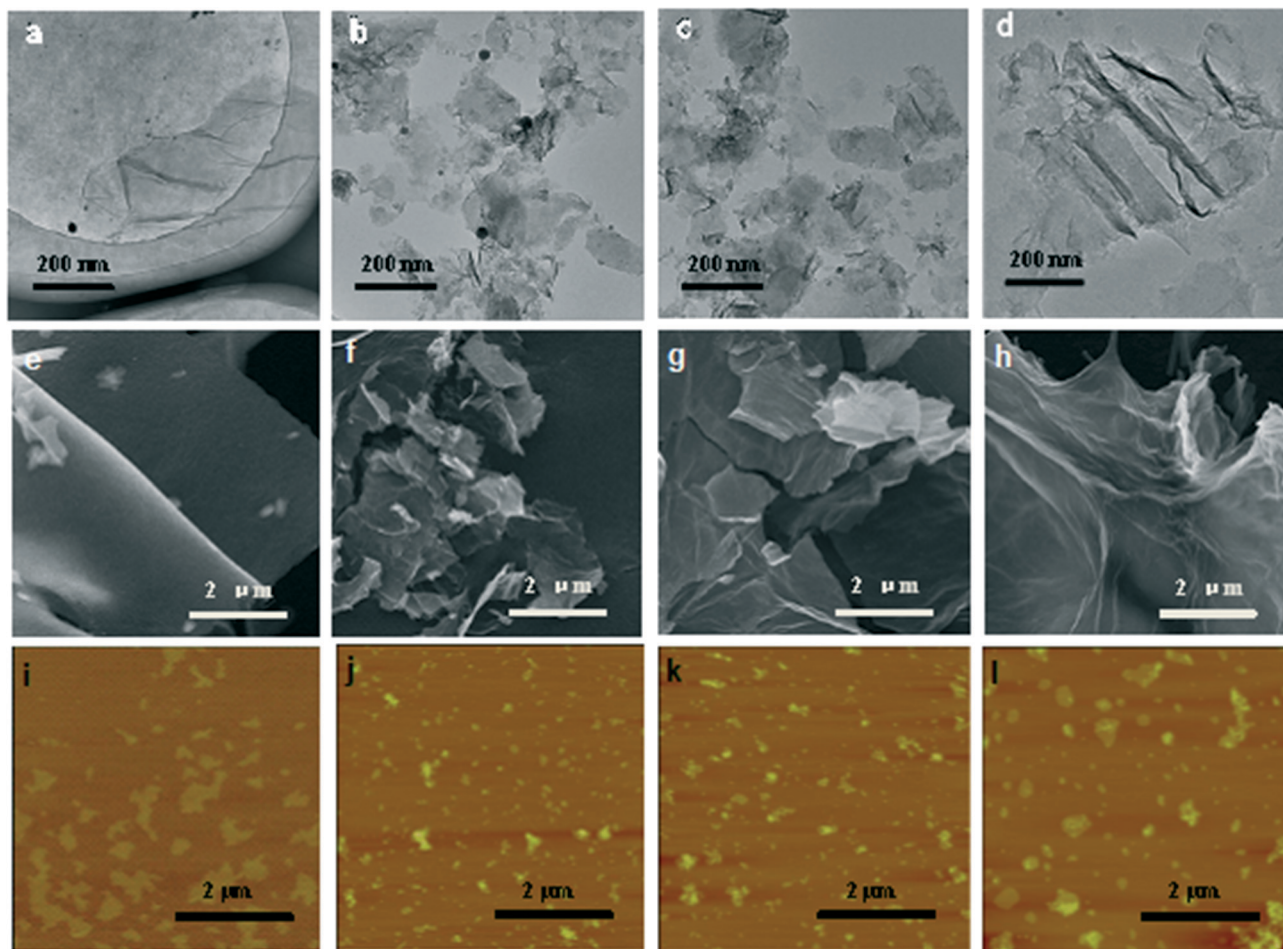


Fig. 2 TEM micrographs of (a) pristine GO, (b)  $\text{GO}_{\text{full}}$ , (c)  $\text{GO}_{\text{UV}}$ , and (d)  $\text{GO}_{\text{vis}}$ . SEM micrographs of (e) pristine GO, (f)  $\text{GO}_{\text{full}}$ , (g)  $\text{GO}_{\text{UV}}$ , and (h)  $\text{GO}_{\text{vis}}$ . AFM images of (i) pristine GO, (j)  $\text{GO}_{\text{full}}$ , (k)  $\text{GO}_{\text{UV}}$ , and (l)  $\text{GO}_{\text{vis}}$ . The irradiation time was 24 h for all the samples.

a sharp decrease in the particle size of  $\text{GO}_{\text{full}}$  and  $\text{GO}_{\text{UV}}$ , indicating that the graphenic sheets of GO were probably cleaved by the UV radiation but the effects of visible light were not as obvious.

### 3.2 Reactive oxygen species (ROS) formation

In this study, three major ROS, *i.e.*,  $^1\text{O}_2$ ,  $\text{O}_2^{\cdot-}$  and  $\cdot\text{OH}$ , were detected when GO was exposed to irradiation at different wavelengths. Fig. 3a shows the steady-state concentration of  $^1\text{O}_2$  generated by GO, a photosensitizer, under different classes of irradiation at pH 7. The results indicate that  $^1\text{O}_2$  could be generated by GO exposed to both UV and visible light. Surprisingly, more  $^1\text{O}_2$  was generated by GO under visible light than UV light, contrary to a previous study which showed a higher production of  $^1\text{O}_2$  by fullerol under UV irradiation compared to visible light.<sup>45</sup> Generally, the energy transfer process leads to the formation of  $^1\text{O}_2$  from the interaction between the excited state of a substance (such as GO) with the ground state of  $\text{O}_2$ . The energy required to promote ground-state  $\text{O}_2$  to  $^1\text{O}_2$  is  $94 \text{ kJ mol}^{-1}$ .<sup>46</sup> Our results indicated that UV and visible light can both excite GO to  $\text{GO}^*$ , which promotes

ground-state  $\text{O}_2$  to  $^1\text{O}_2$  (eqn (5) and (6)). The generation of a smaller amount of  $^1\text{O}_2$  when GO was irradiated with UV light, relative to irradiation with visible light, may be because UV rapidly reduced GO to reduced GO (rGO), resulting in the formation of less  $\text{GO}^*$  and thus a lower production of  $^1\text{O}_2$ .

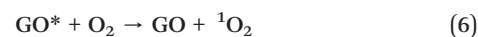


Fig. 3b and c show the steady-state concentrations of  $\text{O}_2^{\cdot-}$  and  $\cdot\text{OH}$  generated by GO. Since  $\text{O}_2^{\cdot-}$  disproportionates rapidly in water to  $\text{H}_2\text{O}_2$ , which is an important precursor for  $\cdot\text{OH}$ , the relative ratio between  $\text{O}_2^{\cdot-}$  and  $\cdot\text{OH}$  may be similar for all light sources.<sup>25</sup> As shown in Fig. 3b and c, the production of  $\text{O}_2^{\cdot-}$  and  $\cdot\text{OH}$  was mainly under UV light. It has been reported that the threshold for GO reduction is 3.2 eV ( $\lambda < 390 \text{ nm}$ ).<sup>47</sup> Based on the literature, the semiconducting domains of GO can act as photocatalysts when irradiated with UV light of energy exceeding the bandgap of the domains.<sup>19</sup> Therefore, UV irradiation of GO results in the formation of electron-hole pairs; the co-occurrence of oxidative (valence

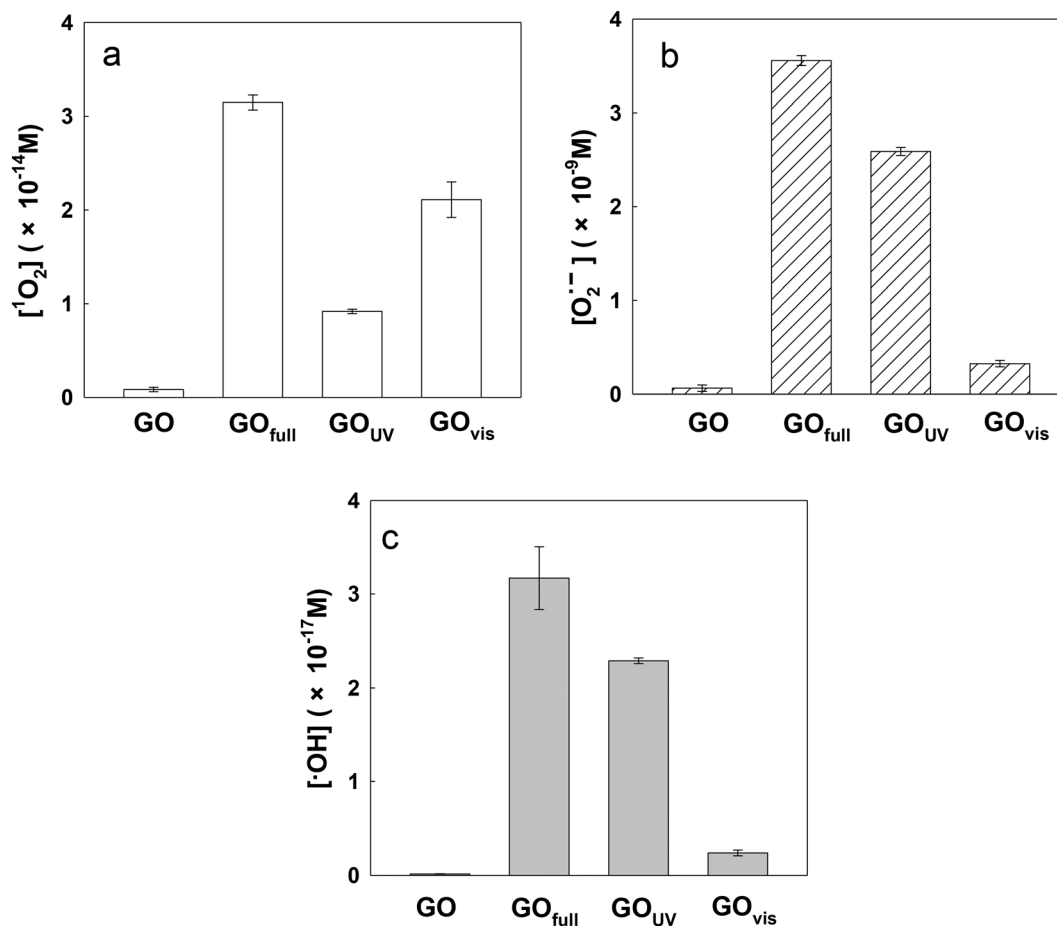
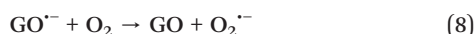


Fig. 3 Steady-state concentrations of (a) singlet oxygen (<sup>1</sup>O<sub>2</sub>), (b) hydroxyl radicals (<sup>•</sup>OH), and (c) superoxide radical anions (O<sub>2</sub><sup>•-</sup>) in GO suspensions in the dark (GO) and exposed to full-spectrum solar (GO<sub>full</sub>), UV (GO<sub>UV</sub>), and visible light (GO<sub>vis</sub>). [GO] = 10 mg L<sup>-1</sup>; pH = 7.

band holes,  $h_{\text{vb}}^+$ ) and reductive (conduction band electron,  $e_{\text{aq}}^-$ ) transients agrees with concurrent GO oxidation and reduction (or disproportionation).<sup>17,48,49</sup> Pickering and Wiesner (2005)<sup>45</sup> hypothesized that irradiation of fullerol led to the formation of the fullerol radical anion, which acted as a precursor for the formation of O<sub>2</sub><sup>•-</sup> via a type I photochemical reaction, and a similar reaction may also occur on the surface of GO. As shown in eqn (7) and (8), the conduction band electron ( $e_{\text{aq}}^-$ ) produced during irradiation of the GO suspension may act as an electron source for the generation of GO radical anions and subsequent formation of O<sub>2</sub><sup>•-</sup>.



It should be noted that the amount of radicals formed by full spectrum irradiation is approximately equal to the amount of radicals formed under UV and visible light combined for all the three ROS determined. This demonstrates the additive effect of light wavelength on ROS production by GO.

### 3.3 Mechanisms controlling GO transformation from UV light, visible light and produced ROS

Of all the ROS, <sup>1</sup>O<sub>2</sub> and O<sub>2</sub><sup>•-</sup> appear to have little effects on GO transformation because of poor oxidation effects. However, <sup>•</sup>OH shows extremely high reactivity and can unselectively react with most organic substances.<sup>25,50</sup> As <sup>•</sup>OH was formed on the surface of GO during the irradiation with UV light, it is possible that <sup>•</sup>OH can attack the surface of GO, similar to the oxidation of the unfunctionalized aromatic ring of small molecular compounds.<sup>51</sup> To understand the effects of <sup>•</sup>OH radicals on the oxidation of GO, we used *tert*-butanol (*t*-BuOH), a scavenger that can selectively eliminate <sup>•</sup>OH radicals in suspension,<sup>52</sup> to further clarify the specific role of <sup>•</sup>OH in the transformation of GO. Fig. 4a–c shows the FTIR spectra of GO under full-spectrum, UV and visible light with or without *t*-BuOH. As shown in the figure, the O-containing functional groups decreased significantly in GO<sub>full</sub> and GO<sub>UV</sub> samples when *t*-BuOH was present, but there was no substantial change for GO<sub>vis</sub>.

Compared with pristine GO (Fig. 1e), FTIR spectroscopy revealed that the O-functional groups changed substantially both without *t*-BuOH (*i.e.*, when both UV light and <sup>•</sup>OH were

active species) and when *t*-BuOH was present (*i.e.*, in the absence of  $\cdot\text{OH}$ ) during UV irradiation, indicating that UV light and  $\cdot\text{OH}$  both have effects on the transformation of GO. The XPS analysis (Fig. 4d–f) further illustrates that  $\cdot\text{OH}$  radicals can hydroxylate GO. Changes in the morphology of GO under UV light with and without *t*-BuOH were compared by TEM, SEM and AFM (Fig. 5). The results clearly show that without  $\cdot\text{OH}$ , GO could hardly be broken into small pieces. This result illustrates that  $\cdot\text{OH}$  may cause the fragmentation of GO.

Based on the results in this study and in the literature,<sup>13,17</sup> we believe that the physicochemical properties of GO are mainly modified by UV light. When GO was irradiated with UV (and full spectrum) light, electron–hole pairs ( $h_{\text{vb}}^+$  and  $e_{\text{aq}}^-$ ) were formed because the photon energy of the light exceeds the bandgap of the domains.<sup>17</sup> Oxidation of O-functional groups on GO by  $h_{\text{vb}}^+$  results in the loss of functional groups and the formation of nanoholes on the surface of GO.  $e_{\text{aq}}^-$  results in the formation of  $\text{GO}^-$  and ROS such as  $\text{O}_2^-$  and  $\cdot\text{OH}$  (Fig. S6†). Furthermore,  $\cdot\text{OH}$  then attacks the surface of GO, leading to the addition of OH groups, as well as the oxidation of C–OH to C=O and O–C=O groups, opening the aromatic rings, fragmenting the GO nanosheets and forming lower molecular weight compounds, as determined from the MS spectra (Fig. S7†).

From these characterization results, we find that the O-containing functional groups on GO did not change significantly under visible light. However, an interesting observation (Fig. 2d and h) was that GO wrinkled significantly during

visible light irradiation, and  $^1\text{O}_2$  formation was also higher than under UV light. Generally, wrinkling of nanostructures typically occurs under aggressive treatment, such as sonication, which may change the structure of the carbon nanosheets.<sup>53</sup> In this study, light irradiation (both UV and visible light) may impact the structure of GO in a similar manner. The energy transfer during visible light irradiation may cause an unbalanced force on the basal plane of GO, leading to wrinkles in the nanomaterials.

In the natural environment, water chemistry factors (such as pH, ionic strength, and natural organic matter (NOM)) as well as turbidity may affect the transformation of GO under different light scenarios. For example, salts and NOM may adsorb onto the surface of GO and prohibit its reduction by light. Very turbid water will most likely absorb light and make it less accessible to the GO particles, which also weakens the reduction of GO. The roles of the physicochemical properties of water on GO transformation under different light conditions, thus, need to be studied further.

### 3.4 Influence of light on the environmental fate of GO

As we have shown, irradiation of GO led to the loss of O-functional groups on the surface of the nanomaterial, which may decrease the hydrophilicity of the nanomaterial in aqueous media. In addition, the morphology of GO was drastically changed, with much smaller sizes observed upon

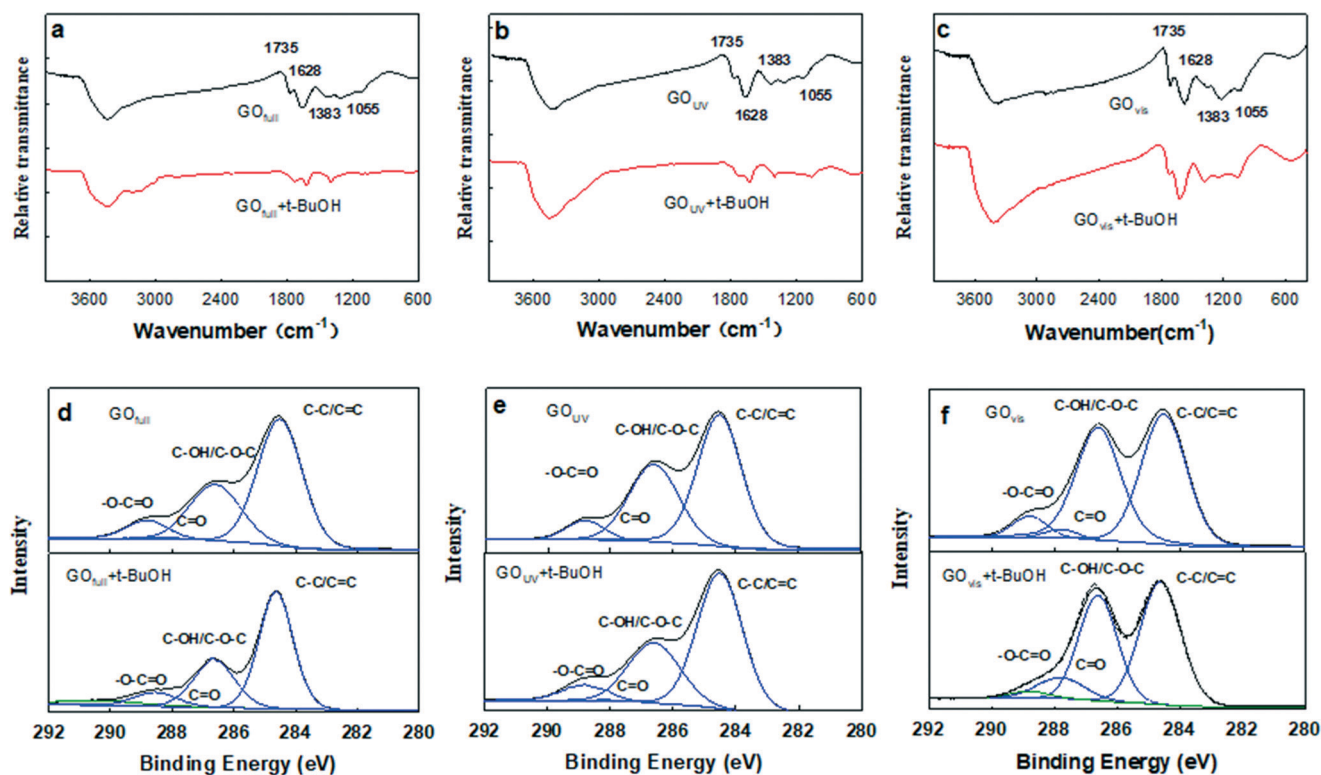


Fig. 4 FTIR spectra of (a) GO<sub>full</sub>, GO<sub>full</sub> with quenching (using *t*-BuOH) (b) GO<sub>UV</sub>, GO<sub>UV</sub> with *t*-BuOH and (c) GO<sub>vis</sub>, GO<sub>vis</sub> with *t*-BuOH; XPS spectra of (d) GO<sub>full</sub>, GO<sub>full</sub> with quenching (*t*-BuOH) (e) GO<sub>UV</sub>, GO<sub>UV</sub> with *t*-BuOH and (f) GO<sub>vis</sub>, GO<sub>vis</sub> with *t*-BuOH.



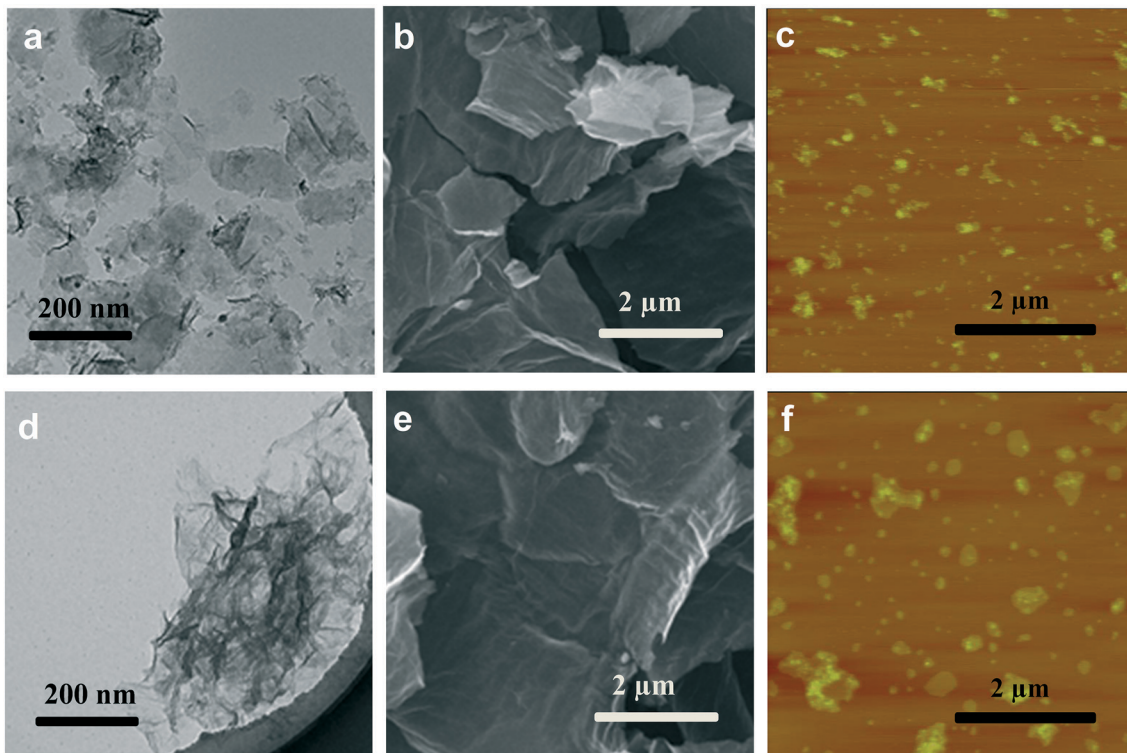


Fig. 5 TEM micrographs, SEM micrographs and AFM images of GO exposed to UV light ( $\lambda = 290\text{--}420\text{ nm}$ ) (a–c) and exposed to UV light with *t*-BuOH (d–f).

irradiation with full-spectrum solar and UV light and sheet wrinkling observed upon irradiation with visible light. All of these light-induced changes may affect the behavior of GO in the natural environment. We, therefore, examined the changes in the electrokinetic properties of GO, induced by different light sources, their effect on agglomeration in aqueous media, and the adsorption affinity of GO for common organic contaminants.

**3.4.1 Zeta ( $\zeta$ ) potential measurements.** The  $\zeta$  potential of GO suspensions exposed to different light sources ( $\text{GO}$ ,  $\text{GO}_{\text{full}}$ ,  $\text{GO}_{\text{UV}}$  and  $\text{GO}_{\text{vis}}$ ) was determined at pH 3 to 11 in order to see the effect of the different irradiation types on the surface charge of the nanomaterial. All four samples were negatively charged across the pH range tested. The  $\zeta$  potentials of  $\text{GO}_{\text{full}}$  and  $\text{GO}_{\text{UV}}$  were comparable, and both were more negative than the  $\zeta$  potential of pristine GO and  $\text{GO}_{\text{vis}}$  (Fig. 6a). GO is negatively charged when dispersed in water due to ionization of the COOH and OH (phenolic) groups.<sup>54,55</sup> The pH of the GO suspension was 4.5. The  $\text{pK}_{\text{a}}$  of the OH group was 9.8, while the  $\text{pK}_{\text{a}}$  of the COOH group was 6.6 when the *ortho* position has no hydroxyl group and 4.3 when there is an OH group present in the *ortho* position. Although there was a net decrease in the oxygen content of GO after treatment with full-spectrum solar and UV light, we observed an increase in the relative abundance of COOH groups in  $\text{GO}_{\text{full}}$  and  $\text{GO}_{\text{UV}}$  (Fig. 1), as explained earlier. The COOH groups observed after irradiation are likely partly those in

close proximity to an OH group, which were reported to be very stable against photodegradation when GO is irradiated.<sup>56</sup> The increased negativity of the  $\zeta$  potential of  $\text{GO}_{\text{full}}$  and  $\text{GO}_{\text{UV}}$  may thus be due to the increased content of COOH groups on GO after UV treatment.<sup>57</sup>

As the acidity of the aqueous medium increased, the  $\zeta$  potential of GO decreased in magnitude, regardless of irradiation treatment, because of the protonation of the OH and COOH groups on GO. In contrast, as the basicity of the suspension media increased we observed an increased negativity due to the presence of negatively charged  $\text{O}^-$  and  $\text{COO}^-$  groups. While the negativity of  $\text{GO}_{\text{full}}$  and  $\text{GO}_{\text{UV}}$  increased more rapidly (than that of pristine GO and  $\text{GO}_{\text{vis}}$ ) between pH 3 and pH 9, GO and  $\text{GO}_{\text{vis}}$  demonstrated a more rapid increase in negativity above pH 9. All these trends show that light of different wavelengths has different impacts on the surface properties of GO in water, which will influence the colloidal behavior of the nanomaterials, as well as its surface interactions with other constituents (organic and inorganic) present in natural waters.

**3.4.2 Agglomeration experiments.** To quantitatively evaluate the effects of different types of irradiation on the colloidal stability of GO in aqueous media, the agglomeration kinetics of  $\text{GO}_{\text{full}}$ ,  $\text{GO}_{\text{UV}}$  and  $\text{GO}_{\text{vis}}$  were studied at 30 mM NaCl. This ionic strength (30 mM) falls within the slow regime for GO agglomeration,<sup>4</sup> where GO undergoes RLCA, allowing for a clear discernment of slight differences in initial

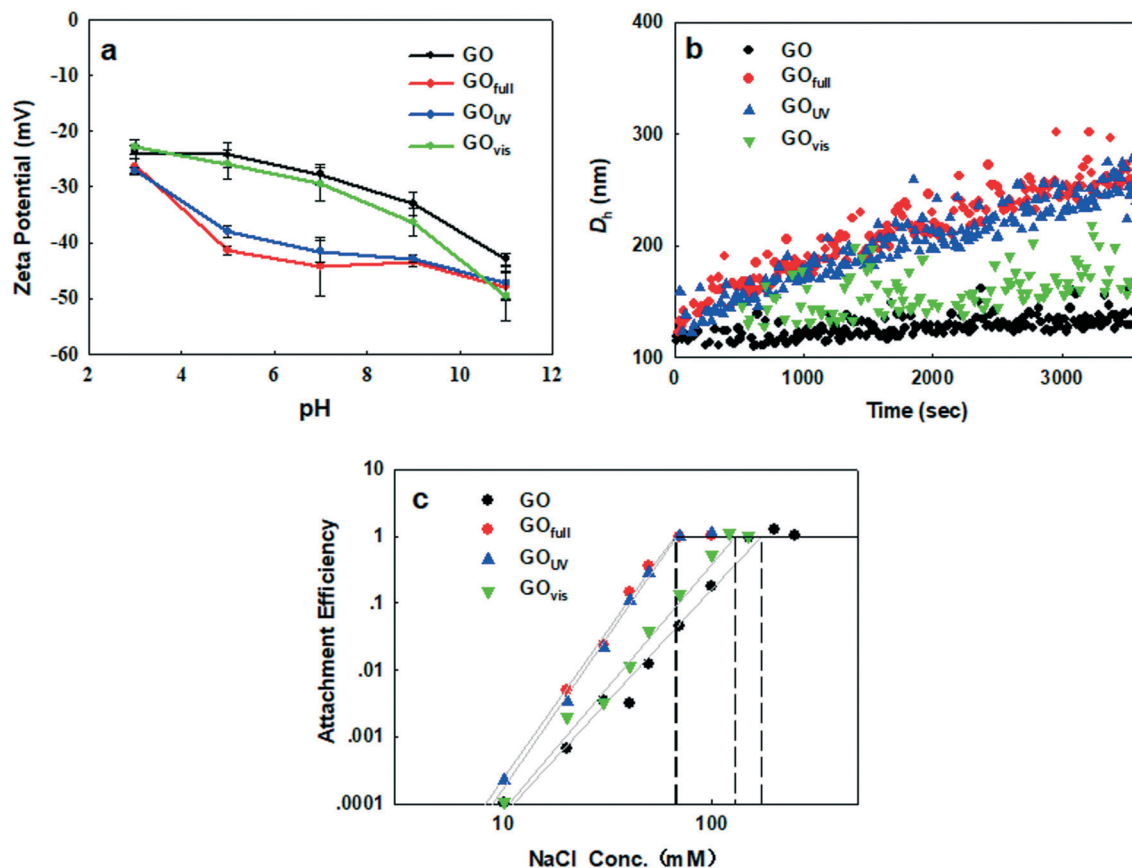


Fig. 6 Influence of different irradiation types on the physicochemical properties of graphene oxide in water. (a) Zeta potential; (b) agglomeration kinetics.  $[\text{Na}^+] = 30 \text{ mg L}^{-1}$ , pH = 7; (c) attachment efficiency as a function of NaCl concentration at pH 7.

agglomeration rate constants,  $k$  (eqn (3)). As shown in Fig. 6b, pristine GO was relatively stable at 30 mM NaCl, with a  $k$  value of  $0.38 \text{ nm min}^{-1}$ . The  $k$  value of GO increased by 48% to  $0.56 \text{ nm min}^{-1}$  when GO was exposed to visible light for 24 h. Irradiation of GO with UV and full-spectrum solar light caused an even more drastic decrease in the colloidal stability of the nanomaterial as  $k$  increased by an order of magnitude to 2.63 and  $5.43 \text{ nm min}^{-1}$ , respectively.

Since the particle size affects the agglomeration rate, we further determined and compared the CCC of the pristine and transformed GO in order to clearly determine how light-induced transformations influence the stability of GO in aqueous media. To achieve this, the changes in the attachment efficiency ( $\alpha$ ) as a function of the NaCl concentration were determined for each GO type. DLCA and RLCA regimes were observed for all four materials, *i.e.* pristine GO, GO<sub>vis</sub>, GO<sub>full</sub> and GO<sub>UV</sub> (Fig. 6c). According to the Derjaguin–Landau–Verwey–Overbeek (DLVO) theory, increasing the ionic strength reduces the electrostatic energy barrier and deepens the secondary minimum well, which promotes agglomeration so that the attachment efficiency gradually increases.<sup>58</sup> As shown in Fig. 6c, the observed CCC values were 171 mM NaCl for GO, 130 mM NaCl for GO<sub>vis</sub>, 67 mM NaCl for GO<sub>UV</sub>, and 66 mM NaCl for GO<sub>full</sub>. This agrees very well with the trend observed in  $k$ , with GO becoming only less stable after visible light treat-

ment but much more unstable when treated with UV and the full light spectrum. In addition, the observed trend in CCC correlates well with the degree of transformation of the GO materials (*i.e.* chemical reduction as indicated by the C/O ratios and size decrease as indicated by AFM) after their exposure to the different light sources. This strongly suggests that the colloidal stability of GO in natural waters is a function of its transformation in the natural environment.

Increased destabilization of GO after UV and full-spectrum solar irradiation could not have been predicted by the  $\zeta$  potential, which, as reported earlier, increased in magnitude under these conditions. The observation of lower colloidal stability of GO<sub>full</sub> and GO<sub>UV</sub>, despite having a higher negative charge on their surfaces compared to pristine GO and GO<sub>vis</sub>, suggests that factors other than electrostatic repulsion played important roles in the agglomeration kinetics of the nanomaterials. We hypothesize that a decrease in the particle size of GO<sub>full</sub> and GO<sub>UV</sub> (as shown by electron microscopy and AFM in Fig. 2), a decrease in the van der Waals force, and an increase in the hydrophobic effect led to their increased agglomeration. A decrease in particle size changes the structure and surface energy characteristics of nanomaterials, which may impact the total potential energy of interaction.<sup>59</sup> Meanwhile, van der Waals forces and hydrophobic effect may also have effects on the GO agglomeration.

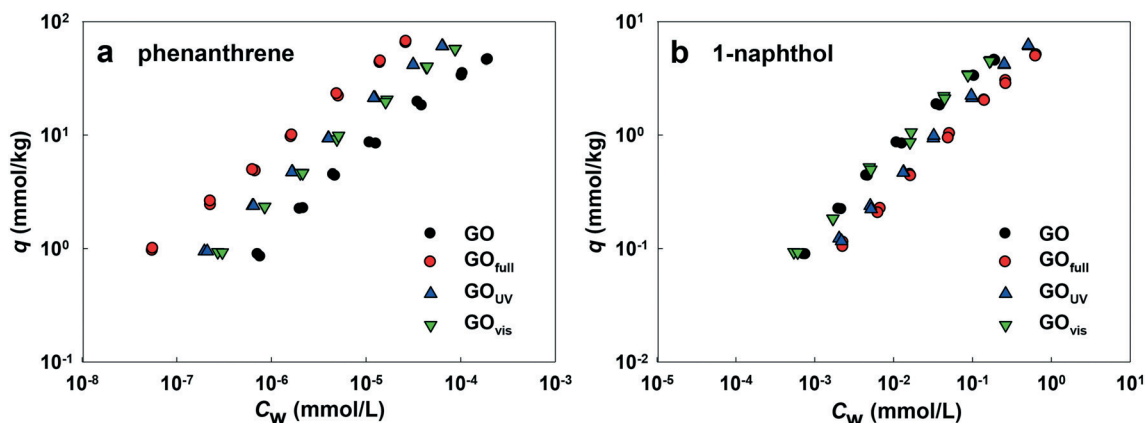


Fig. 7 Isotherms of adsorption of phenanthrene (a) and 1-naphthol (b) onto the colloidal GO,  $GO_{full}$ ,  $GO_{UV}$  and  $GO_{vis}$  suspensions;  $q$  ( $\text{mmol kg}^{-1}$ ) and  $C_w$  ( $\text{mmol L}^{-1}$ ) are the equilibrium concentrations of an adsorbate on GO and in the solution, respectively.

Using the classical DLVO theory, He *et al.* (2008)<sup>59</sup> showed that the interaction potential decreases as the particle size decreases, leading to increased agglomeration of smaller-sized nanomaterials. Also, smaller GO particles possess a higher fraction of their atoms on the edges, which may increase the density of active sites. A higher density of active sites and a larger specific surface area of smaller-sized GO can enhance the interaction with counterions in the surrounding media, leading to decreased colloidal stability. The van der Waals force between  $GO_{full}$  and  $GO_{UV}$  samples increased due to the decrease in particle size. However, as the van der Waals force is weak, it probably has only slight effects on the interaction of the GO particles. On the other hand, the hydrophobic effect may be much more important. As O-functional groups decreased and the C/O ratio increased for  $GO_{full}$  and  $GO_{UV}$  samples, the hydrophobic effect may be substantially increased, promoting the agglomeration of GO particles.

**3.4.3 Adsorption experiments.** The isotherms of adsorption of phenanthrene and 1-naphthol onto pristine GO,  $GO_{full}$ ,  $GO_{UV}$  and  $GO_{vis}$  are shown in Fig. 7a and b. The adsorption data were fitted with the Freundlich adsorption model:  $q = K_F \times C_w^n$ . ( $q$ : the equilibrium concentration of an adsorbate on GO;  $C_w$ : the equilibrium concentration of an adsorbate in the solution;  $K_F$ : the Freundlich affinity coefficient;  $n$ : the Freundlich linearity index).

Fig. 7a shows the adsorption affinities of GO for phenanthrene. The results indicate that adsorption was enhanced with irradiation from all light sources. The adsorption isotherms of  $GO_{full}$ ,  $GO_{UV}$  and  $GO_{vis}$  were substantially shifted compared with the isotherm obtained for pristine GO. This demonstrates that the adsorption of PAHs onto GO is mainly driven by hydrophobic effects and particle size.<sup>60,61</sup> Thus, the reduction of the surface O-containing functional groups of GO by full-spectrum and UV light irradiation could affect the adsorption of phenanthrene due to increased surface hydrophobicity and decreased particle size (which may result in higher surface area). Surprisingly, the adsorption affinity of  $GO_{vis}$  was also increased, even as much as  $GO_{UV}$ . As no obvi-

ous chemical change was observed on the surface of  $GO_{vis}$ , the increased adsorption of phenanthrene may be due to the wrinkles formed on the surface of  $GO_{vis}$ , which created additional sites for phenanthrene attachment.

Fig. 7b shows that the adsorption affinity of GO for 1-naphthol was also enhanced after light irradiation, but the extent of adsorption enhancement was much less compared with phenanthrene. This is mainly because the  $\log K_{OW}$  value of 1-naphthol (2.85) is much less than that of phenanthrene (4.57), and the aqueous solubility of 1-naphthol ( $3.04 \text{ mmol L}^{-1}$ ) is much greater than that of phenanthrene ( $6.31 \times 10^{-3} \text{ mmol L}^{-1}$ ).<sup>37</sup> Hence, the mechanisms controlling the adsorption of 1-naphthol and phenanthrene onto GO are different. The results indicate that adsorption of 1-naphthol onto GO is strongly affected by hydrogen bonding between the OH group of 1-naphthol and the surface O-functionalities of GOs,<sup>62</sup> as well as the  $\pi$ - $\pi$  interactions. As such, the adsorption of 1-naphthol by  $GO_{UV}$  and  $GO_{full}$  decreased because of the loss of OH groups upon irradiation.

## 4 Conclusions

Release of GO materials into surface water will facilitate some physicochemical transformations by light irradiation. As shown in this study, the O-containing functional groups of GO are decreased by UV irradiation (or the UV fraction of solar light). These chemical changes lead to physical variation in the nanosheets—mainly cleavage of the GO nanosheets. The  $\cdot\text{OH}$  radicals, which are formed during UV irradiation, are also involved in the transformation of GO, hydroxylating the surface of GO, as well as breaking up the GO nanosheets into small pieces. Visible light (or the visible range of solar light) can hardly alter the chemical composition of GO but changes the appearance of GO and wrinkled the GO nanosheets. The transformation of GO by light may be affected by water chemistry. The chemical changes in GO, especially the loss of O-containing functional groups, is the main factor which affects the agglomeration of GO, while the changes in GO morphology and hydrophobicity strongly affect the adsorption of hydrophobic organic pollutants.

## Conflicts of interest

The authors declare that they have no conflicts of interest.

## Acknowledgements

This research was supported by the National Basic Research Program of China (Grant 2014CB932001 and Grant 2015CB459000), the National Natural Science Foundation of China (Project No. 21677078), the 111 Program, Ministry of Education, China (Grant T2017002), and the Basic Scientific Research Program (Grant 7954).

## References

- 1 D. R. Dreyer, S. Park, C. W. Bielawski and R. S. Ruoff, The chemistry of graphene oxide, *Chem. Soc. Rev.*, 2010, **39**, 228–240.
- 2 W. Gao, L. B. Alemany, L. Ci and P. M. Ajayan, New insights into the structure and reduction of graphite oxide, *Nat. Chem.*, 2009, **1**, 403–408.
- 3 D. G. Goodwin, Jr., A. S. Adeleye, L. Sung, K. T. Ho, R. M. Burgess and E. J. Petersen, Detection and quantification of graphene-family nanomaterials in the environment, *Environ. Sci. Technol.*, 2018, **52**, 4491–4513.
- 4 I. Chowdhury, M. C. Duch, N. D. Mansukhani, M. C. Hersam and D. Bouchard, Colloidal properties and stability of graphene oxide nanomaterials in the aquatic environment, *Environ. Sci. Technol.*, 2013, **47**, 6288–6296.
- 5 Y. Li, J. Yang, Q. Zhao and Y. Li, Dispersing carbon-based nanomaterials in aqueous phase by graphene oxides, *Langmuir*, 2013, **29**, 13527–13534.
- 6 A. S. Adeleye, J. R. Conway, K. Garner, Y. Huang, Y. Su and A. A. Keller, Engineered nanomaterials for water treatment and remediation: Costs, benefits, and applicability, *Chem. Eng. J.*, 2016, **286**, 640–662.
- 7 K. Krishnamoorthy, K. Jeyasubramanian, M. Premanathan, G. Subbiah, H. S. Shin and S. J. Kim, Graphene oxide nanopaint, *Carbon*, 2014, **72**, 328–337.
- 8 R. Song, Y. Qin, S. Suh and A. A. Keller, Dynamic model for the stocks and release flows of engineered nanomaterials, *Environ. Sci. Technol.*, 2017, **51**, 12424–12433.
- 9 S. C. Ray, in *Applications of Graphene and Graphene-Oxide Based Nanomaterials*, William Andrew Publishing, Oxford, 2015, pp. 39–55, DOI: 10.1016/B978-0-323-37521-4.00002-9.
- 10 T. Du, Y. Wang, X. Yang, W. Wang, H. Guo, X. Xiong, R. Gao, X. Wuli, A. S. Adeleye and Y. Li, Mechanisms and kinetics study on the trihalomethanes formation with carbon nanoparticle precursors, *Chemosphere*, 2016, **154**, 391–397.
- 11 T. Du, A. S. Adeleye, A. A. Keller, Z. Wu, W. Han, Y. Wang, C. Zhang and Y. Li, Photochlorination-induced transformation of graphene oxide: Mechanism and environmental fate, *Water Res.*, 2017, **124**, 372–380.
- 12 L. Duan, R. Hao, Z. Xu, X. He, A. S. Adeleye and Y. Li, Removal of graphene oxide nanomaterials from aqueous media via coagulation: Effects of water chemistry and natural organic matter, *Chemosphere*, 2017, **168**, 1051–1057.
- 13 W.-C. Hou, W. M. Henderson, I. Chowdhury, D. G. Goodwin, Jr., X. Chang, S. Martin, D. H. Fairbrother, D. Bouchard and R. G. Zepp, The contribution of indirect photolysis to the degradation of graphene oxide in sunlight, *Carbon*, 2016, **110**, 426–437.
- 14 Y. Li, N. Yang, T. Du, X. Wang and W. Chen, Transformation of graphene oxide by chlorination and chloramination: Implications for environmental transport and fate, *Water Res.*, 2016, **103**, 416–423.
- 15 F. Wang, F. Wang, G. Gao and W. Chen, Transformation of graphene oxide by ferrous iron: Environmental implications, *Environ. Toxicol. Chem.*, 2015, **34**, 1975–1982.
- 16 T. Xia, J. D. Fortner, D. Zhu, Z. Qi and W. Chen, Transport of sulfide-reduced graphene oxide in saturated quartz sand: Cation-dependent retention mechanisms, *Environ. Sci. Technol.*, 2015, **49**, 11468–11475.
- 17 W.-C. Hou, I. Chowdhury, D. G. Goodwin, Jr., W. M. Henderson, D. H. Fairbrother, D. Bouchard and R. G. Zepp, Photochemical transformation of graphene oxide in sunlight, *Environ. Sci. Technol.*, 2015, **49**, 3435–3443.
- 18 Y. Matsumoto, M. Koinuma, S. Y. Kim, Y. Watanabe, T. Taniguchi, K. Hatakeyama, H. Tateishi and S. Ida, Simple photoreduction of graphene oxide nanosheet under mild conditions, *ACS Appl. Mater. Interfaces*, 2010, **2**, 3461–3466.
- 19 Y. Matsumoto, M. Koinuma, S. Ida, S. Hayami, T. Taniguchi, K. Hatakeyama, H. Tateishi, Y. Watanabe and S. Amano, Photoreaction of graphene oxide nanosheets in water, *J. Phys. Chem. C*, 2011, **115**, 19280–19286.
- 20 M. Tedetti and R. Sempere, Penetration of ultraviolet radiation in the marine environment. A review, *Photochem. Photobiol.*, 2006, **82**, 389–397.
- 21 E. W. Helbling, K. S. Gao, R. J. Goncalves, H. Y. Wu and V. E. Villafane, Utilization of solar UV radiation by coastal phytoplankton assemblages off SE China when exposed to fast mixing, *Mar. Ecol.: Prog. Ser.*, 2003, **259**, 59–66.
- 22 H. Piazena, E. Perez-Rodrigues, D. P. Hader and F. Lopez-Figueroa, Penetration of solar radiation into the water column of the central subtropical Atlantic Ocean - optical properties and possible biological consequences, *Deep Sea Res., Part II*, 2002, **49**, 3513–3528.
- 23 Q. Zhao, C. Shang, X. Zhang, G. Ding and X. Yang, Formation of halogenated organic byproducts during medium-pressure UV and chlorine coexposure of model compounds NOM and bromide, *Water Res.*, 2011, **45**, 6545–6554.
- 24 A. S. Adeleye, X. Wang, F. Wang, R. Hao, W. Song and Y. Li, Photoreactivity of graphene oxide in aqueous system: Reactive oxygen species formation and bisphenol A degradation, *Chemosphere*, 2018, **195**, 344–350.
- 25 D. Zhang, S. Yan and W. Song, Photochemically induced formation of reactive oxygen species (ROS) from effluent organic matter, *Environ. Sci. Technol.*, 2014, **48**, 12645–12653.
- 26 V. C. Tung, M. J. Allen, Y. Yang and R. B. Kaner, High-throughput solution processing of large-scale graphene, *Nat. Nanotechnol.*, 2009, **4**, 25–29.

- 27 D. E. Latch, B. L. Stender, J. L. Packer, W. A. Arnold and K. McNeill, Photochemical fate of pharmaceuticals in the environment: Cimetidine and ranitidine, *Environ. Sci. Technol.*, 2003, **37**, 3342–3350.
- 28 M. Sahni and B. R. Locke, Quantification of hydroxyl radicals produced in aqueous phase pulsed electrical discharge reactors, *Ind. Eng. Chem. Res.*, 2006, **45**, 5819–5825.
- 29 J. D. Fortner, D.-I. L. Kim, A. M. Boyd, J. C. Falkner, S. Moran, V. L. Colvin, J. B. Hughes and J.-H. Kim, Reaction of Water-Stable C<sub>60</sub> aggregates with ozone, *Environ. Sci. Technol.*, 2007, **41**, 7497–7502.
- 30 S. Kim and W. Choi, Kinetics and mechanisms of photocatalytic degradation of (CH<sub>3</sub>)<sub>n</sub>NH<sub>4-n</sub><sup>+</sup> (0 ≤ n ≤ 4) in TiO<sub>2</sub> suspension: The role of OH radicals, *Environ. Sci. Technol.*, 2002, **36**, 2019–2025.
- 31 K. L. Chen and M. Elimelech, Influence of humic acid on the aggregation kinetics of fullerene (C<sub>60</sub>) nanoparticles in monovalent and divalent electrolyte solutions, *J. Colloid Interface Sci.*, 2007, **309**, 126–134.
- 32 A. S. Adeleye, J. R. Conway, T. Perez, P. Rutten and A. A. Keller, Influence of extracellular polymeric substances on the long-term fate, dissolution, and speciation of copper-based nanoparticles, *Environ. Sci. Technol.*, 2014, **48**, 12561–12568.
- 33 A. S. Adeleye and A. A. Keller, Interactions between algal extracellular polymeric substances and commercial TiO<sub>2</sub> nanoparticles in aqueous media, *Environ. Sci. Technol.*, 2016, **50**, 12258–12265.
- 34 A. S. Adeleye and A. A. Keller, Long-term colloidal stability and metal leaching of single wall carbon nanotubes: Effect of temperature and extracellular polymeric substances, *Water Res.*, 2014, **49**, 236–250.
- 35 A. S. Adeleye, S. Pokhrel, L. Maedler and A. A. Keller, Influence of nanoparticle doping on the colloidal stability and toxicity of copper oxide nanoparticles in synthetic and natural waters, *Water Res.*, 2018, **132**, 12–22.
- 36 V. Runkana, P. Somasundaran and P. C. Kapur, Reaction-limited aggregation in presence of short-range structural forces, *AIChE J.*, 2005, **51**, 1233–1245.
- 37 F. Wang, F. Wang, D. Zhu and W. Chen, Effects of sulfide reduction on adsorption affinities of colloidal graphene oxide nanoparticles for phenanthrene and 1-naphthol, *Environ. Pollut.*, 2015, **196**, 371–378.
- 38 X. Li, W. Chen, C. Zhang, Y. Li, F. Wang and W. Chen, Enhanced dehydrochlorination of 1,1,2,2-tetrachloroethane by graphene-based nanomaterials, *Environ. Pollut.*, 2016, **214**, 341–348.
- 39 C. Nethravathi, T. Nisha, N. Ravishankar, C. Shivakumara and M. Rajamathi, Graphene-nanocrystalline metal sulphide composites produced by a one-pot reaction starting from graphite oxide, *Carbon*, 2009, **47**, 2054–2059.
- 40 S. Park, K. Lee, G. Bozoklu, W. Cai, S. T. Nguyen and R. S. Ruoff, Graphene oxide papers modified by divalent ions - Enhancing mechanical properties via chemical cross-linking, *ACS Nano*, 2008, **2**, 572–578.
- 41 C. Rodriguez-Gonzalez, A. L. Martinez-Hernandez, V. M. Castano, O. V. Kharissova, R. S. Ruoff and C. Velasco-Santos, Polysaccharide nanocomposites reinforced with graphene oxide and keratin-grafted graphene oxide, *Ind. Eng. Chem. Res.*, 2012, **51**, 3619–3629.
- 42 L. Guardia, S. Villar-Rodil, J. I. Paredes, R. Rozada, A. Martinez-Alonso and J. M. D. Tascon, UV light exposure of aqueous graphene oxide suspensions to promote their direct reduction, formation of graphene-metal nanoparticle hybrids and dye degradation, *Carbon*, 2012, **50**, 1014–1024.
- 43 M. S. Dresselhaus, A. Jorio, M. Hofmann, G. Dresselhaus and R. Saito, Perspectives on carbon nanotubes and graphene Raman spectroscopy, *Nano Lett.*, 2010, **10**, 751–758.
- 44 L. Szpyrkowicz, C. Juzzolino and S. N. Kaul, A comparative study on oxidation of disperse dyes by electrochemical process, ozone hypochlorite and Fenton reagent, *Water Res.*, 2001, **35**, 2129–2136.
- 45 K. D. Pickering and M. R. Wiesner, Fullerol-sensitized production of reactive oxygen species in aqueous solution, *Environ. Sci. Technol.*, 2005, **39**, 1359–1365.
- 46 F. Wilkinson, W. P. Helman and A. B. Ross, Quantum yields for the photosensitized formation of the lowest electronically excited singlet state of molecular oxygen in solution, *J. Phys. Chem. Ref. Data*, 1993, **22**, 113–262.
- 47 V. A. Smirnov, A. A. Arbutov, Y. M. Shul'ga, S. A. Baskakov, V. M. Martynenko, V. E. Muradyan and E. I. Kresova, Photoreduction of graphite oxide, *High Energy Chem.*, 2011, **45**, 57–61.
- 48 H. Xu, W. J. Cooper, J. Jung and W. Song, Photosensitized degradation of amoxicillin in natural organic matter isolate solutions, *Water Res.*, 2011, **45**, 632–638.
- 49 Y. Zhang, L. Guo, H. Xia, Q. Chen, J. Feng and H. Sun, Photoreduction of graphene oxides: Methods, properties, and applications, *Adv. Opt. Mater.*, 2014, **2**, 10–28.
- 50 M. O. Buffle, S. Galli and U. von Gunten, Enhanced bromate control during ozonation: The chlorine-ammonia process, *Environ. Sci. Technol.*, 2004, **38**, 5187–5195.
- 51 J. Yao, Z. Huang and S. J. Masten, The ozonation of pyrene: Pathway and product identification, *Water Res.*, 1998, **32**, 3001–3012.
- 52 J. Staehelin and J. Hoigne, Decomposition of ozone in water in the presence of organic solutes acting as promoters and inhibitors of radical chain reactions, *Environ. Sci. Technol.*, 1985, **19**, 1206–1213.
- 53 M. V. Savoskin, V. N. Mochalin, A. P. Yaroshenko, N. I. Lazareva, T. E. Konstantinova, I. V. Barsukov and L. G. Prokofiev, Carbon nanoscrolls produced from acceptor-type graphite intercalation compounds, *Carbon*, 2007, **45**, 2797–2800.
- 54 D. Li, M. B. Mueller, S. Gilje, R. B. Kaner and G. G. Wallace, Processable aqueous dispersions of graphene nanosheets, *Nat. Nanotechnol.*, 2008, **3**, 101–105.
- 55 T. Szabo, O. Berkesi, P. Forgo, K. Josepovits, Y. Sanakis, D. Petridis and I. Dekany, Evolution of surface functional

- groups in a series of progressively oxidized graphite oxides, *Chem. Mater.*, 2006, **18**, 2740–2749.
- 56 B. Konkana and S. Vasudevan, Engineering a water-dispersible, conducting photoreduced graphene oxide, *J. Phys. Chem. C*, 2015, **119**, 6356–6362.
- 57 B. Konkana and S. Vasudevan, Understanding aqueous dispersibility of graphene oxide and reduced graphene oxide through  $pK_a$  measurements, *J. Phys. Chem. Lett.*, 2012, **3**, 867–872.
- 58 M. Elimelech, J. Gregory, X. Jia and R. A. Williams, in *Particle Deposition and Aggregation*, ed. M. Elimelech, J. Gregory, X. Jia and R. A. Williams, Butterworth-Heinemann, 1995, pp. 310–343, DOI: 10.1016/B978-0-7506-0743-8.50015-7.
- 59 Y. T. He, J. Wan and T. Tokunaga, Kinetic stability of hematite nanoparticles: The effect of particle sizes, *J. Nanopart. Res.*, 2008, **10**, 321–332.
- 60 J. Wang, Z. Chen and B. Chen, Adsorption of polycyclic aromatic hydrocarbons by graphene and graphene oxide nanosheets, *Environ. Sci. Technol.*, 2014, **48**, 4817–4825.
- 61 J. Xu, L. Wang and Y. Zhu, Decontamination of bisphenol A from aqueous solution by graphene adsorption, *Langmuir*, 2012, **28**, 8418–8425.
- 62 Z. Pei, L. Li, L. Sun, S. Zhang, X. Shan, S. Yang and B. Wen, Adsorption characteristics of 1,2,4-trichlorobenzene, 2,4,6-trichlorophenol, 2-naphthol and naphthalene on graphene and graphene oxide, *Carbon*, 2013, **51**, 156–163.